



## RESEARCH LETTER

10.1002/2016GL072415

## Key Points:

- Maximum earthquake magnitude increases with the width of the seismogenic zone and is unaffected by subduction velocity
- Seismic rate increases with subduction velocity; rate of the largest events increases with subduction velocity/seismogenic zone width ratio
- Random sampling shows that poor correlations in nature may be due to too short observations

## Supporting Information:

- Supporting Information S1

## Correspondence to:

F. Corbi,  
fabio.corbi3@gmail.com

## Citation:

Corbi F., R. Herrendörfer, F. Fucicello, and Y. van Dinther (2017), Controls of seismogenic zone width and subduction velocity on interplate seismicity: Insights from analog and numerical models, *Geophys. Res. Lett.*, *44*, 6082–6091, doi:10.1002/2016GL072415.

Received 21 DEC 2016

Accepted 28 APR 2017

Accepted article online 3 MAY 2017

Published online 28 JUN 2017

## Controls of seismogenic zone width and subduction velocity on interplate seismicity: Insights from analog and numerical models

Fabio Corbi<sup>1</sup> , Robert Herrendörfer<sup>2</sup> , Francesca Fucicello<sup>3</sup> , and Ylona van Dinther<sup>2</sup> 

<sup>1</sup>Géosciences Montpellier Laboratory, University of Montpellier, Montpellier, France, <sup>2</sup>Institute of Geophysics, ETH Zurich, Zurich, Switzerland, <sup>3</sup>Dipartimento di Scienze, Roma Tre University, Rome, Italy

**Abstract** Correlations between geodynamic parameters and interplate seismicity characteristics in subduction zones are generally weak due to the short instrumental record and multiparameter influences. To investigate the role of subduction velocity  $V_s$  and the width of the seismogenic zone  $W$  on maximum magnitude  $M_{\max}$ , seismic rate  $\tau$ , characteristic recurrence rate  $\tau_c$ , and moment release rate  $MRR$ , we use synthetic data sets from simplified analog and numerical models to gain insight into natural subduction zones seismicity. Our models suggest that  $M_{\max}$  increases with  $W$  and is unaffected by  $V_s$ ,  $\tau$  increases with  $V_s$ ,  $\tau_c$  increases with  $V_s/W$ , and  $MRR$  increases with  $V_s \times W$ . In nature, only the positive correlation between  $V_s$  and  $\tau$  is significant. Random sampling of our time series suggest that the positive correlation between  $V_s$  and  $\tau$  can be observed with short observation time windows. Other correlations, including  $M_{\max}$  versus  $W$ , become clear only for time window lengths longer than  $1/\tau_c$ .

### 1. Introduction

The world's largest earthquakes occur along the subduction megathrusts: the large faults between the subducting and overriding plates (Figure 1a). Along megathrusts, stress is locally built up as a consequence of friction that acts against plate convergence. When the fault strength is overcome, stress is released through a variety of slip modes that range from slow slip events to regular earthquakes [e.g., *Ide et al.*, 2007; *Schwartz and Rokosky*, 2007; *Peng and Gombert*, 2010]. During regular earthquakes, slip can quickly reach tens of meters and involve hundreds of kilometers of the fault, resulting in moment magnitude  $M_w$  8 or larger earthquakes. These earthquakes, in combination with tsunamis that they may trigger, can cause extensive human losses and severe damages in densely populated areas, as for the 2011  $M_w$  9.0 Tohoku-Oki event (Japan).

The seismic signature differs between subduction zones under various aspects, including the maximum magnitude and earthquake productivity [e.g., *Ide*, 2013]. Such variability has been initially attributed to the combination of age of subducting plate and plate-rate convergence [*Uyeda and Kanamori*, 1979; *Ruff and Kanamori*, 1980]. However, this former idea failed in explaining the occurrence of events like the 2004 Sumatra and the 2011 Tohoku-Oki, pushing the scientific community to find other possible links between subduction interplate seismicity and long-term geodynamic parameters [e.g., *Heuret et al.*, 2011; *Schellart and Rawlinson*, 2013].

Two parameters, namely, the downdip width of the seismogenic zone  $W$  and subduction velocity  $V_s$ , have been proposed to exert a key role on interplate seismicity for their first-order control on deformation rate and coupling area between plates, respectively [e.g., *Kanamori and Brodsky*, 2001; *Scholz and Campos*, 2012]. However, previous studies focusing on the possible relationships between seismicity and  $W$  or  $V_s$  lead to contradicting conclusions. While *Kelleher et al.* [1974] concluded that the maximum magnitude increases with the width of the contact zone between the converging plates, *Pacheco et al.* [1993] and *Heuret et al.* [2011] found no significant correlation between these two parameters. Similarly for  $V_s$ , *Ruff and Kanamori* [1980] and *Jarrard* [1986] noted that the earthquake magnitude potential of subduction zones is positively correlated with relative plate motions, but then it is not clear why the fastest subduction zones (i.e., Tonga and the New Hebrides) have not experienced a  $M_w > 8.0$  earthquake along the megathrust since 1900 [e.g., *Heuret et al.*, 2011].

These observational studies provide a snapshot of an intertwined truth, as they are confronted with a too short instrumental time span within which multiple, intercorrelated geodynamic parameters affect the

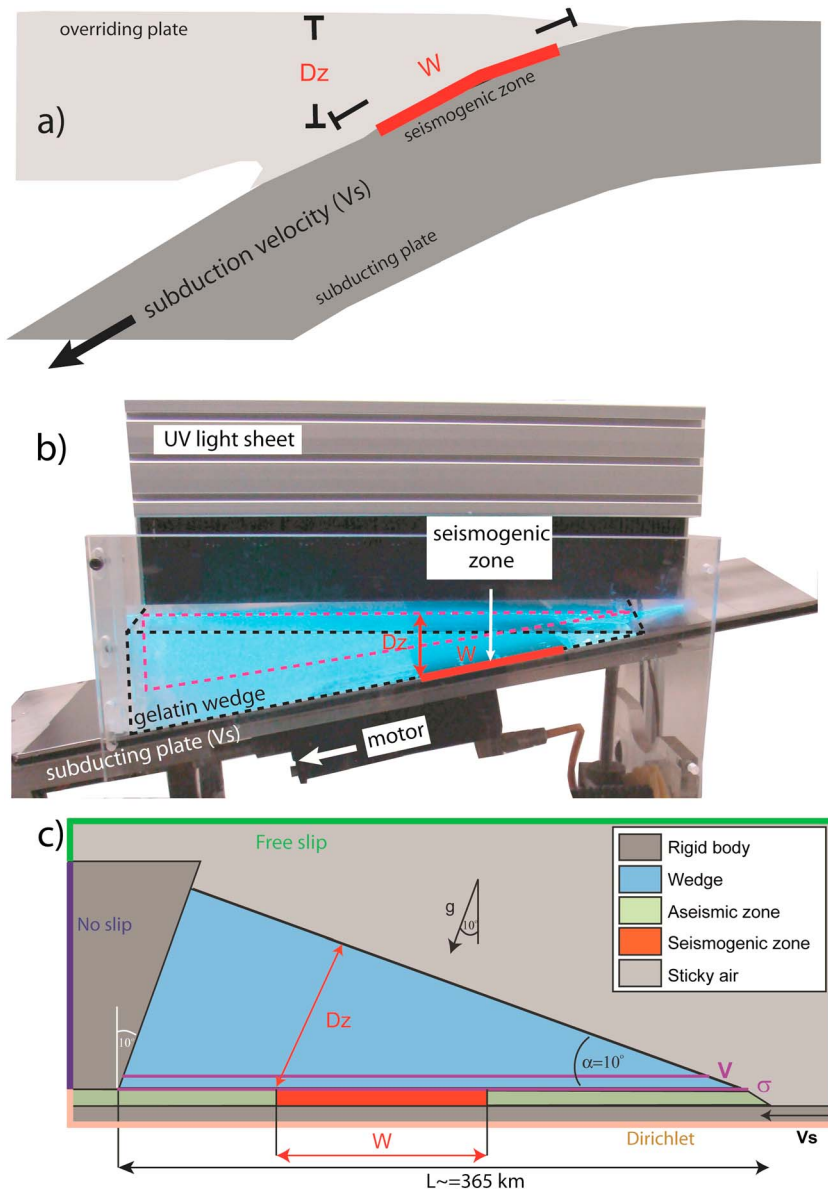


**Figure 1.** Schematic representation of a subduction zone in (a) nature compared to our (b) analog and (c) numerical models. The red lines highlight the seismogenic zone. The dashed purple polygon in Figure 2b highlights the cross-sectional area analyzed by PIV. The numerical setup, including gravity vector, is rotated by the subduction angle of  $10^\circ$  with respect to the analog setup. Boundary conditions are given in the respective sides.

seismicity at the same time. Our instrumental record dates back to 1900, while thousands of years of data are required to cover several complete seismic cycles and reveal each subduction zone seismic characteristics [e.g., McCaffrey, 2008]. Unfortunately, paleoseismological investigations [e.g., Cisternas et al., 2005; Sieh et al., 2008] do not provide enough spatiotemporal coverage to extend our global analysis that far back in time. Additionally, contemporary variations of several geodynamic parameters within tens of subduction zones make it difficult to identify one-to-one correlations and cause-effect relationships [e.g., Heuret et al., 2011].

To overcome these limitations, we use complementary analog and numerical models to investigate how  $W$  and  $V_s$  control the seismic behavior of subduction interplate events. Both analog and numerical models have recently become a robust tool of investigation [e.g., Corbi et al., 2013; van Dinther et al., 2013a, 2013b, 2014; Funiello et al., 2013; Rosenau et al., 2009; Herrendörfer et al., 2015]. Their main advantage is the capability to simulate tens to hundreds of seismic cycles per model. Properly scaled analog models are physically

self-consistent (i.e., stresses and strain evolve spontaneously in response to applied boundary conditions), while numerical models have also the advantage of being more flexible and efficient for a parametric study. A previous benchmark ensures the similarity between the two modeling techniques [van Dinther *et al.*, 2013a]. To describe the seismic behavior of our models, we use the following parameters: maximum magnitude  $M_{\max}$ , seismic rate  $\tau$ , characteristic seismic rate  $\tau_c$  [Herrendörfer *et al.*, 2015], and moment release rate  $MRR$  (supporting information Text S1). These parameters allow us to answer the following questions: (a) how large is the strongest event? (b) how many events occur in a given time period? (c) what is the recurrence time of the largest events? and (d) how fast is the release of seismic energy for a given (geometric and kinematic) subduction configuration in a given time window? We finally compare the modeling results with a database that includes geometrical, mechanical, and seismological properties of worldwide subduction zones [Heuret *et al.*, 2011]. The aim of this comparison is to identify potential cause-effect relationships among the investigated parameters that may be flawed by the short observation interval and multiparameter influence.

## 2. Methods

We use three complementary sources of information to analyze the role of  $W$  and  $V_s$ . Besides a global database of natural subduction zones [Heuret *et al.*, 2011], new insights are provided by a systematic parameter study executed with analog and numerical models that have been described in detail by Corbi *et al.* [2013] and van Dinther *et al.* [2013a, 2013b], respectively. Here we recall their basics, while a summary of model performance and scaling is provided in supporting information Text S2. The setup of our models (Figures 1b and 1c) mimics the subduction environment (Figure 1a). A  $10^\circ$  dipping, flat and undeformable plate, analog of the downgoing slab, underthrusts a viscoelastic wedge (i.e., the overriding plate). The frictional interaction between converging plates leads to a stress buildup, which is episodically released by frictional instabilities propagating along the base of the model (i.e., the analog earthquakes). A velocity-weakening zone (analog of the seismogenic zone) is confined between two velocity-strengthening zones at its updip and downdip limits [e.g., Scholz, 1998; Marone and Saffer, 2007].  $V_s$  is applied as a boundary condition in the numerical model and via a stepping motor in the analog models.  $W$  is varied together with the depth  $D_z$  of the downdip limit according to the worldwide geometry of subduction zones (supporting information Figure S1 and Table S1). The numerical models systematically investigate the role of  $D_z$  at constant  $V_s$ . Since  $D_z$  plays only a secondary role on the selected seismological parameters, related results are shown in supporting information Text S3. The numerical models are 2-D and the analog models are quasi-2-D as the geometric, kinematic, and frictional properties of the setup are constant along the width. The trench-parallel extent of the analog model is 34 cm, but a UV lamp is used to lighten a few millimeters thin section of the model. Both analog and numerical models are monitored for a time scaled to nature of  $>10^5$  years, allowing to recognize tens of seismic cycles per model.

Correlations between the investigated parameters (i.e.,  $W$  and  $V_s$ ) and seismological ones (i.e.,  $M_{\max}$ ,  $\tau$ , and  $MRR$ ) are provided by means of Spearman correlation coefficient  $R$  and  $p$  value [Press *et al.*, 1996] both for our models and for natural subduction zones ( $R$  and  $p$  values are reported within individual plots of Figures 2, 3, and S4). The Spearman correlation coefficient is a nonparametric measurement that indicates how well two variables follow a monotonic function. With respect to the more common Pearson correlation coefficient, the Spearman correlation coefficient has the advantage of dealing with skewed data or outliers. This is particularly important for the natural data set where correlations may be flawed by few fast subduction zones (i.e., North Tonga and New Hebrides) [Heuret *et al.*, 2011].

### 2.1. Analog Models

The wedge is made of 2.5 wt % Pig Skin gelatin (see Di Giuseppe *et al.* [2009] for details on rheological properties and preparation and Corbi *et al.* [2011] for frictional behavior of gel against sandpaper). The seismogenic zone is modeled with sandpaper, while the updip and downdip velocity-strengthening zones are modeled with acetate plastic sheets. The setup is designed maintaining  $D_z$  constant during the experimental run. Monitoring is performed via particle image velocimetry (PIV) method (MatPIV) [Sveen, 2004]. The velocity field is used to calculate model deformation time series and earthquake source parameters [Corbi *et al.*, 2013].

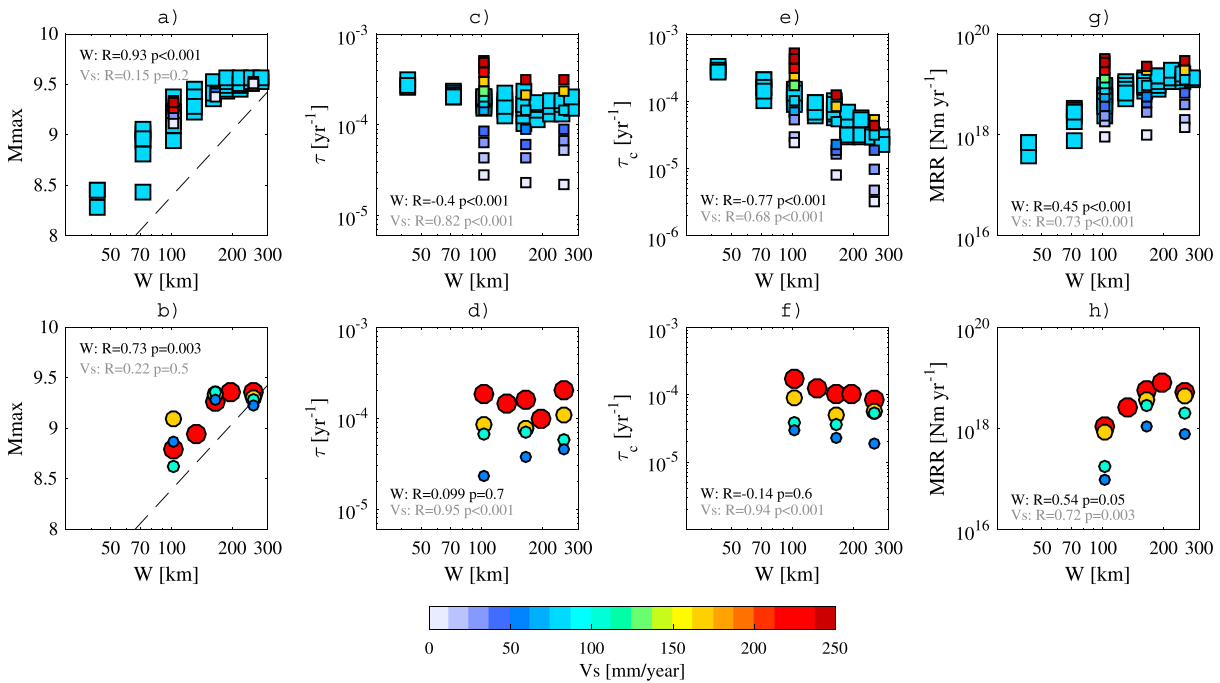


**Figure 2.** Modeling results: (a and b) Maximum magnitude  $M_{max}$ , (c and d) seismic rate  $\tau$ , (e and f) characteristic rate  $\tau_c$ , and (g and h) moment release rate  $MRR$  as a function of  $W$  and  $V_s$  (color bar) in numerical models (Figures 2a, 2c, 2e, and 2g) and analog models (Figures 2b, 2d, 2f, and 2h). The black dashed line in Figures 2a and 2b represents the  $M_w-R_w$  scaling [Blaser et al., 2010] for  $R_w = W$ .

**2.2. Numerical Models**

The continuum-mechanics-based numerical model solves for the conservation equations of mass and momentum for an incompressible medium with a visco-elasto-plastic rheology [Gerya and Yuen, 2007]. The governing equations are discretized on a fully staggered finite difference grid in combination with a marker-in-cell technique, in which advected markers carry material properties. The interface between the wedge and the subducting plate is modeled as a frictional boundary layer, in which a nonassociative Drucker-Prager plastic flow law is applied with a pressure-dependent yield strength. To simulate analog

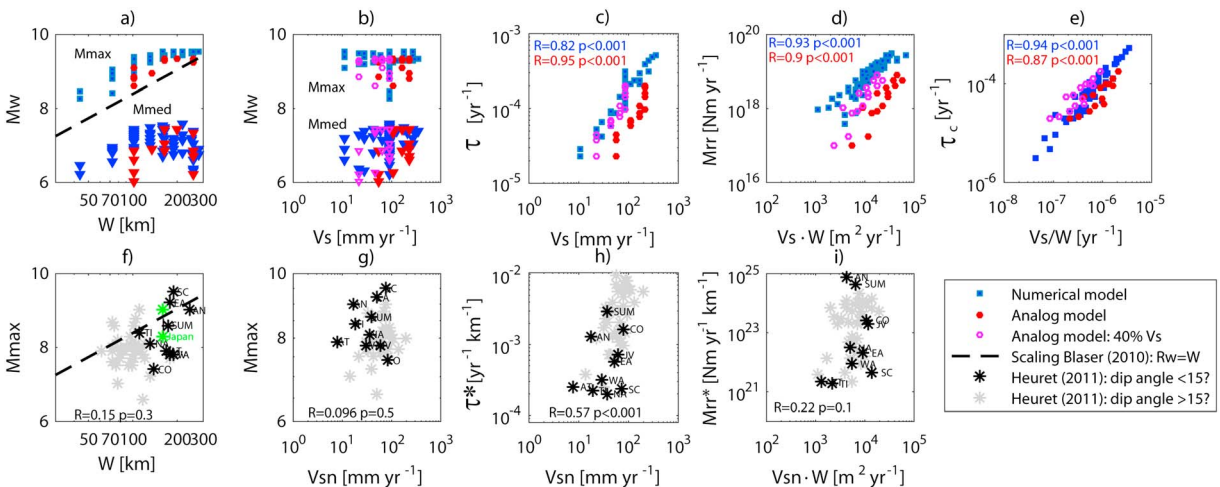


**Figure 3.** Summarized role of  $W$  and  $V_s$  on the (a and b) maximum (squares) and medium magnitude (triangles). (c) Role of  $V_s$  on  $\tau$ . (d) Control of  $V_s \times W$  on  $MRR$  and (e) control of  $V_s/W$  on  $\tau_c$ . The roles of  $W$  and  $V_{sn}$  in the data set of natural subduction zones [Heuret et al., 2011] are shown for comparison in terms of (f and g)  $M_{max}$ , (h)  $\tau$ , and (i)  $MRR$ . Each panel reports the Spearman correlation coefficient  $R$  and the  $p$  value. Subduction zones with a dip angle  $\leq 15^\circ$ : Sumatra (SUM), Cocos (CO), Andaman (AN), Java (JV), E-Alaska (EA), Western Aegean (WA), Antilles (AT), Timor (TI), Nankai (NA), and Southern Chile (SC). Green stars in Figure 3f represent  $M_{max}$  for the Japan subduction zone segment before (i.e.,  $M_w = 8.3$ ) and after the 2011  $M_w = 9.0$  Tohoku earthquake, respectively.

earthquakes, *van Dinther et al.* [2013a, 2013b] introduced a velocity-dependent friction and the inertial term to the momentum equations (see also supporting information Text S4 for numerical details and Table S2 for the list of material properties).

### 2.3. Natural Database

We compare modeling results with the natural global database compiled by *Heuret et al.* [2011]. This database includes  $M_w \geq 5.5$  interplate events that occurred worldwide in the 1976–2007 interval sampled from the Harvard centroid moment tensor catalog [*Dziwonski and Woodhouse, 1981*], including the 2010 Maule  $M_w$  8.8 earthquake, and  $M_w > 7$  in the 1900–1975 interval sampled from the Centennial catalog [*Engdahl and Villaseñor, 2002*]. The 2011 Tohoku  $M_w$  9.0 is not included in the database; however, we discuss its impact on  $M_{\max}$ . Besides seismological information, the database includes  $W$  and  $V_s$  of worldwide subduction zones. As our models have a subduction angle of  $10^\circ$ , we highlight the subsample of the original database with shallowly dipping seismogenic zones (dip angle  $< 15^\circ$ ).

## 3. Results and Analysis

### 3.1. Control on $M_{\max}$

In our analog and numerical models,  $M_{\max}$  overall increases with  $W$  (Figures 2a and 2b and 3a and 3b). The largest events rupture at least the entire seismogenic zone width (i.e., a rupture width equal or larger than  $W$ , dashed line in Figures 2a and 2b) and also propagate into the updip and downdip velocity-strengthening regions. This penetration distance depends on the frictional properties along the plate interface and the downdip location of the seismogenic zone with respect to the trench and backstop. For  $W > 180$  km,  $M_{\max}$  saturates at  $M_w \sim 9.5$ . This first-order control of  $W$  on the size of the rupture and, therefore, on the maximum seismic moment leads to high correlations between  $M_{\max}$  and  $W$ . In contrast to  $W$ ,  $M_{\max}$  is mostly insensitive to  $V_s$ , leading to insignificant correlations between  $M_{\max}$  and  $V_s$  (Figures 2a and 2b and 3a and 3b). The reason is that  $V_s$  does not affect the size of the coupling area between the plates along which a slip deficit can be accumulated and released.

### 3.2. Control on $\tau$ and $\tau_c$

In our models, the seismic rate  $\tau$  increases mainly as a function of  $V_s$  as  $V_s$  controls the slip deficit accumulation rate in the seismogenic zone. Consequently, correlations between  $V_s$  and  $\tau$  are high (Figures 2c and 2d and 3c).

$\tau_c$ —the recurrence rate of the characteristic events—clearly decreases as a function of  $W$  in the numerical models, while the correlation between the same parameters appears weaker in the analog models. The correlation is affected by the analog experiments that have the widest seismogenic zones. In these analog models, the simulated time series are not long enough to capture the recurrence time of the largest events such that the characteristic recurrence time rate reflects the shorter recurrence time of smaller events.  $\tau_c$  clearly increases as a function of  $V_s$  both in the numerical and analog models (Figures 2e and 2f).

As shown above,  $W$  determines primarily the maximum slip area, while  $V_s$  controls the rate at which the slip deficit is built up along that area. Therefore, the inverse of the ratio between  $V_s/W$  yields the time until the seismogenic zone is fully loaded and the largest event can be generated. Therefore,  $V_s/W$  is expected to control  $\tau_c$ , which is confirmed by high correlations between  $V_s/W$  and  $\tau_c$  both in the analog and numerical model (Figure 3e).

### 3.3. Control on $MRR$

In our models,  $MRR$  increases both with  $V_s$  and  $W$  (Figures 2g and 2h). Similarly to  $M_{\max}$ ,  $MRR$  increases with  $W$  for  $W < 180$  km due to the strong influence of the increasing rupture width of the largest earthquakes in wider seismogenic zones. For  $W > 180$  km  $MRR$  approaches our setup's limit of  $M_{\max}$ . Similarly to  $\tau$  and  $\tau_c$ ,  $MRR$  is affected by the role of  $V_s$  in controlling the stress and slip deficit built-up rate, which leads to high correlations between  $V_s$  and  $MRR$ .

The combination of the roles of  $V_s$  and  $W$  as  $V_s \times W$  multiplied with the constant shear modulus  $GG$  in our models yields a 2-D seismic moment accumulation rate and, hence, leads to the expectation that this

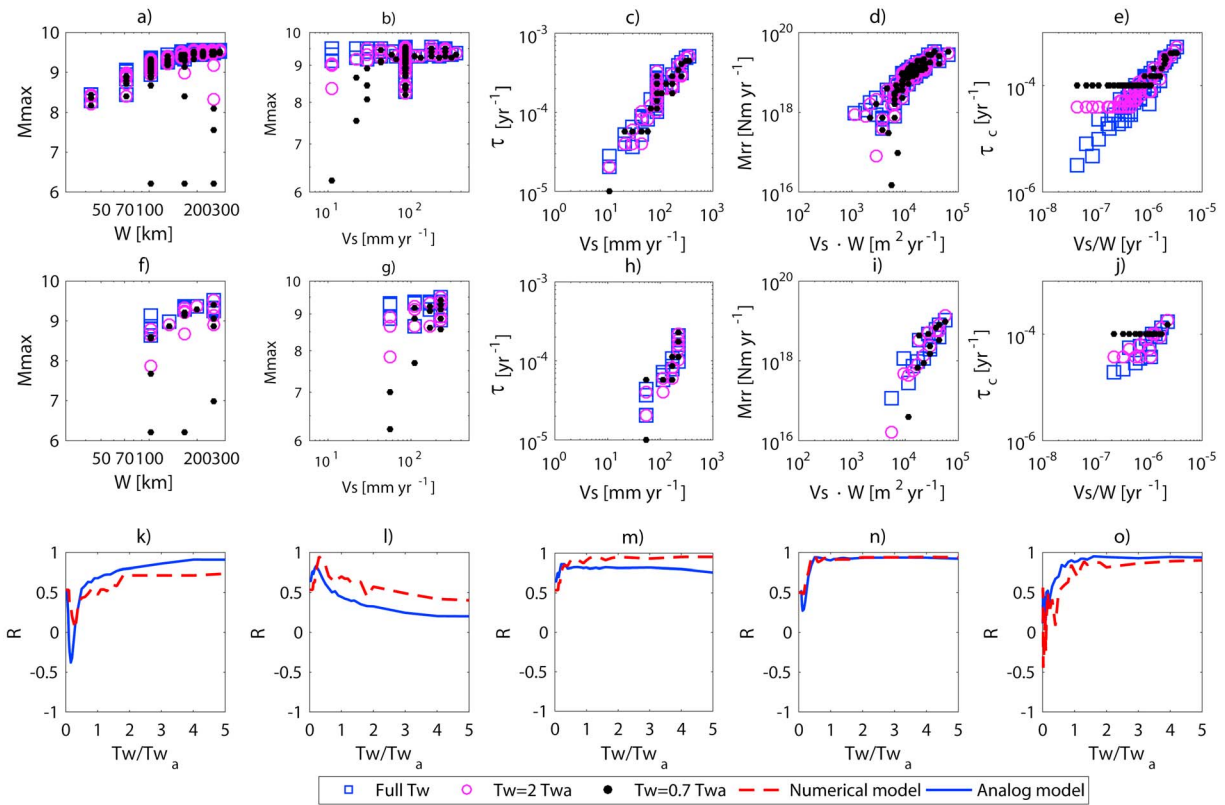


**Figure 4.** (a–j) Median of selected parameters for various time window lengths (reported in legend). (k–o) Variation of the Spearman’s correlation coefficient  $R$  as a function of normalized time window length  $T_w/T_{w_a}$ . For the purpose of visualization in the log-log plot, a fixed value of rupture width = 10 km ( $M_w = 6.2$ ) and  $MRR = 10^{15}$  Nm/s and  $\tau = 10^{-5}$  is assigned to a random time window if it does not contain any event. Furthermore, if no characteristic pattern occurs in the random time window, the characteristic recurrence time is equal to the time window length. Figures 4a–4e and 4f–4j refer to numerical and analog models, respectively. Figures 4k–4o show the  $R$  values for the set of parameters in the respective column.

moment accumulation rate controls at first-order  $MRR$ . This expectation is confirmed by high correlations between  $V_s \times W$  and  $MRR$  in our models (Figure 3d).

### 3.4. Role of Interseismic Locking

Results show that  $\tau$ ,  $MRR$ , and  $\tau_c$  are lower in the analog than in the numerical model for a given  $V_s$ ,  $V_s \times W$  and  $V_s/W$ , respectively (Figures 3c–3e). It was noticed that the interseismic locking in the analog models is lower (~40%) than in the numerical models (~100%) [van Dinther et al., 2013a, 2013b; Corbi et al., 2013]. This affects the slip deficit accumulation rate at a given  $V_s$ , thereby reducing the impact of  $V_s$  on  $\tau$ ,  $MRR$ , and  $\tau_c$  discussed above. Accounting for the difference in interseismic locking (i.e., reducing  $V_s$  by 40% in the analog models) results in a better agreement between numerical and analog model results (Figures 3c–3e).

### 3.5. Correlations in Nature and Impact of the Time Window Length

In nature, correlations between  $V_s$ ,  $W$ , or a combination of both with the investigated seismic quantities are weak (Figures 3f–3i). One exception is the high correlation between  $V_s$  and  $\tau$  (Figure 3h).

To better understand what causes the weak correlations in nature, we quantified in our models how the estimate of  $M_{max}$ ,  $\tau$ ,  $MRR$ , and  $\tau_c$  and their correlations with  $V_s$ ,  $W$ , or a combination of both is affected by the observation time window length  $T_w$ . We sampled the time series with 100 time windows with random initial beginnings. From these 100 random time windows, we calculated the median value of each quantity. This analysis is conducted for a range of time window lengths  $T_w$ .

For  $T_w = 0.7 \times T_{w_a}$  ( $T_{w_a} = 25$  kyr is the average characteristic recurrence time of the numerical and analog models), correlations are different than for the full time window (Figure 4) with the exception

of the high correlation between  $V_s$  versus  $\tau$  (Figures 4c, 4h, and 4m) and between  $V_s \times W$  and  $MRR$  (Figures 4d, 4i, and 4n).  $M_{\max}$  is strongly underestimated, and  $\tau_c$  is not determinable in models with long characteristic recurrence times (i.e., large  $W$  and low  $V_s$ ; Figures 4a, 4b, 4f, and 4g). This leads to a low correlation between  $M_{\max}$  and  $W$  and between  $V_s/W$  and  $\tau_c$ . The high correlations determined at full time windows are approached for  $Tw > 2 Tw_a$  (Figures 4k and 4o).  $Tw = 0.7 Tw_a$  also produces a positive apparent high correlation between  $V_s$  and  $M_{\max}$ , which is strongly reduced for longer  $Tw$  (Figure 4l). In models with low  $V_s$  and large  $W$ ,  $MRR$  deviates from the clear relationship between  $V_s \times W$  and  $MRR$  due to the slow moment accumulation rate and the long recurrence time of characteristic events.

#### 4. Discussion

The combination of our models with natural observations, each with their own nonoverlapping uncertainties and limitations (supporting information Text S5), leads to the following discussion points.

Our models show that  $M_{\max}$  is mainly controlled by  $W$  as the rupture potential increases with  $W$ . This is in agreement with studies suggesting that a large downdip extent of the seismogenic zone is required for the occurrence of mega events [Kelleher *et al.*, 1974; Uyeda and Kanamori, 1979; Lay *et al.*, 1982]. In our models, the largest ruptures saturate the entire seismogenic zone and propagate into the velocity-strengthening regions, resulting in  $M_{\max}$  larger than those predicted by simple magnitude - rupture width  $R_w$  scaling for  $R_w = W$  [Blaser *et al.*, 2010]. The location of  $M_{\max}$  of several subduction zones (e.g., East Alaska and Japan; Figure 3f) above this  $M_w$ - $W$  scaling suggests  $M_{\max}$  may exceed the magnitude based on this scaling in nature. Regarding the rupture potential to propagate outside the seismogenic zone, an alternative mechanism to the inefficient arresting effect of velocity-strengthening regions observed in our models is dynamic fault weakening, as suggested for the 2011  $M_w$  9.0 Tohoku earthquake [Noda and Lapusta, 2013].

Random sampling of our time series suggests that an observation history longer than the characteristic recurrence time (i.e.,  $= 1/\tau_c$ ) is needed to constrain real  $M_{\max}$  for a given subduction zone, and  $Tw > 2 Tw_a$  to obtain high correlations between  $M_{\max}$  and  $W$  (Figures 4a, 4f, and 4k). A similar conclusion (i.e.,  $Tw > 5$  times the characteristic recurrence time) for determining the recurrence time of  $M_w > 9$  events was constrained statistically for natural megathrust earthquakes [McCaffrey, 2008]. This limited observation span with respect to the seismic cycle duration might explain: (a) why  $M_{\max}$  for the majority of natural subduction zones is smaller than  $M_{\max}$  predicted on the base of  $M_w$ - $W$  scaling (Figure 3e) and (b) why the observed  $M_{\max}$  of the majority of subduction zones are more similar to the median magnitude of our models (Figure 3a). A striking example is the 2011  $M$  9.0 Tohoku earthquake with a rupture width of 200 km [Romano *et al.*, 2014]. Before this event, the instrumentally recorded  $M_{\max}$  on the Japan segment was 8.3, which is lower than expected from its  $W = 161$  km [Heuret *et al.*, 2011] (Figure 3e). It should be noted, however, that by using the scaling law [Blaser *et al.*, 2010], we assume that  $M_{\max}$  scales with  $R_w$ . Although a large downdip  $R_w$  is linked to a wide along-strike rupture lengths [e.g., Wells and Coppersmith, 1994], it is debatable whether this scaling law holds at very high  $M_w$  since unrealistically high widths would be expected for  $M_w > 9.2$ . Such great megathrust earthquakes have a large along-strike component (e.g., the 2004 Sumatra-Andaman earthquake) [Shearer and Bürgmann, 2010], which is not taken into account in our 2-D models. Therefore,  $M_{\max}$  might be controlled by other factors that have been suggested to control the along-strike rupture propagation, such as the trench-parallel extent of a subduction zone segment, the upper plate strain [Heuret *et al.*, 2012], interplate roughness [e.g., Wang and Bilek, 2014], and megathrust curvature [Schellart and Rawlinson, 2013; Blettery *et al.*, 2016].

In our models as well as in natural subduction zones, no significant correlation between  $M_{\max}$  and  $V_s$  is obtained (Figures 2a and 2b and 3b and 3g). Based on natural observations, it is unclear whether  $V_s$  individually controls  $M_{\max}$ . On one hand, Heuret *et al.* [2011] identified a feedback between slow subduction zones, shallow dipping slab, and wide seismogenic zones, which is proposed to lead to the generation of the largest  $M_{\max}$ . On the other hand, Uyeda [1983] associated the largest magnitudes with fast subduction zones due to their high mechanical coupling of the subduction megathrust. In our models high  $V_s$  is associated to high  $\tau$  and  $\tau_c$  increasing the probability to observe the largest events. Random sampling of our

time series shows that at short time window lengths an apparent positive correlation between  $V_s$  and  $M_{\max}$  is found in contrast to the low correlation found at longer time windows (Figure 4l). Therefore, previously suggested  $M_{\max}$ - $V_s$  correlations for nature might have been affected by this potential observational bias. This is in agreement with statistical simulations suggesting that the occurrence of  $M_w > 9$  earthquakes cannot be excluded at any subduction zone, independently of  $V_s$  [McCaffrey, 2008]. However, it should be noted that our models do not take into account the thermal evolution of a subduction zone, which is suggested to control the vertical extent of the seismogenic zone [e.g., Heuret et al., 2011; Dal Zilio et al., 2016]. More complete physical models that self-consistently resolve both subduction dynamics and seismogenesis are thus required to provide further insights.

$V_s$  is found to exert a primary control on  $\tau$  and  $\tau_c$  both in analog and in numerical models, which supports the direct correlation between  $V_s$  and  $\tau$  that is found when considering subduction megathrust events only [e.g., Heuret et al., 2011] and the whole convergent margin seismicity [Ide, 2013]. When taking the different interseismic locking in the analog and numerical models into account, the  $\tau$  versus  $V_s$  and  $MRR$  versus  $V_s \times W$  relationships of both models tend to overlap (Figures 3c and 3d). The reduced interseismic locking in the analog models may be explained by creeping that occurs at the base of the gelatin wedge, which in turn reduces the seismic coupling. Natural subduction zones display a wide range of seismic coupling [e.g., Scholz and Campos, 2012], whose calculation is, however, affected by the short observation time. Moreover, interseismic locking may also change through subsequent seismic cycles as suggested for the Mentawai segment of the Sunda megathrust [Philibosian et al., 2014]. Aseismic slip transients belonging to the slow slip phenomena observed in subduction zones [e.g., Peng and Gomberg, 2010] release periodically a fraction of the accumulated elastic energy of convergent margins and thereby reduce the long-term locking [e.g., Radiguet et al., 2016]. Therefore, different sources affecting the amount of locking in subduction zones may explain the scatter of  $\tau$  and  $V_s$  in the natural database (Figure 3h).

In our models,  $MRR$  is controlled by both  $V_s$  and  $W$  (Figures 2g and 2h). In nature,  $MRR$  is mainly influenced by the contribution of the largest event. For example, the great 1960  $M_w$  9.5 Chile earthquake alone accounts for about 30% of the total seismic energy released during the last century [Heuret et al., 2011]. Our models furthermore demonstrate that the frequency of the largest events is a crucial factor to estimate the long-term  $MRR$ . This frequency,  $\tau_c$ , is shown to be controlled by the ratio of  $V_s/W$ , which means that larger  $W$  reduces the recurrence rate of the largest events. This weakens the positive impact of  $W$  on  $MRR$  (Figure 3e). Consequently, the fastest subduction zones with medium to large  $W$  are expected to have the largest  $MRR$ . A comparison of the correlations with respect to  $MRR$  and  $\tau_c$  would require multiple cycles of the largest events, which is clearly beyond the available data. Paleoseismological studies [e.g., Cisternas et al., 2005; Sieh et al., 2008] might provide such estimates in some subduction zones to allow for a comparison in future studies.

## 5. Conclusions

The following conclusions are drawn linking our analog and numerical models to natural observations:

1.  $M_{\max}$  increases with  $W$ , which suggests that subduction zones with the largest observed rupture widths smaller than  $W$  have shown only a fraction of their seismic potential.
2. Our models show no cause-effect relationship between  $V_s$  and  $M_{\max}$ .
3.  $V_s$  determines the slip deficit accumulation rate. Thereby, it controls  $\tau$ .
4.  $V_s \times W$  determines the moment accumulation rate, which in turn controls  $MRR$ .
5.  $W$  does not play a relevant role in controlling  $\tau$  in our models and in nature, but our models suggest that  $V_s/W$  controls  $\tau_c$ .
6. Different interseismic locking between our analog and numerical models affects  $\tau$ ,  $MRR$ , and  $\tau_c$ . This suggests that differences in interseismic locking can explain part of the scattered relationship between  $V_s$  and  $\tau$  and between  $V_s$  and  $MRR$  in nature.
7. Random sampling of our time series suggests that (a) high correlations between  $M_{\max}$  and  $W$ ,  $V_s/W$ , and  $\tau_c$  become only observable for time window lengths larger than the characteristic recurrence time; (b) the previously observed correlation between  $V_s$  and  $M_{\max}$  in nature is due to the short observation interval; and (c) the high correlation between  $V_s$  and  $\tau$ , also observed in nature, and between  $V_s \times W$  and  $MRR$  can be observed with short time windows.

## Acknowledgments

F.C. and R.H. ran and analyzed the analog and numerical models, respectively, while together taking the lead in paper writing. All authors contributed into concept development and further writing of the paper. Riccardo Lanari is acknowledged for his support in the laboratory. Serge Lallemand is acknowledged for fruitful discussions on a preliminary version of the manuscript. We thank W. Schellart and an anonymous reviewer for the constructive review of the paper. F.C. received funding from the European Union's Horizon 2020 research and innovation program under the Marie Skłodowska-Curie grant agreement 658034 (AspSync). R.H. was supported by SNSF grant 200021-153524. Analog and numerical modeling data are available by contacting the corresponding author and R.H. (robert.herrendoerfer@erdw.ethz.ch), respectively.

## References

- Blaser, L., F. Krüger, M. Ohrnberger, and F. Scherbaum (2010), Scaling relations of earthquake source parameter estimates with special focus on subduction environment, *Bull. Seismol. Soc. Am.*, *100*(6), 2914–2926, doi:10.1785/0120100111.
- Bletery, Q., A. M. Thomas, A. W. Rempel, L. Karlstrom, A. Sladen, and L. De Barros (2016), Mega-earthquakes rupture flat megathrusts, *Science*, *354*(6315), 1027–1031, doi:10.1126/science.aag0482.
- Cisternas, M., et al. (2005), Predecessors of the giant 1960 Chile earthquake, *Nature*, *437*(7057), 404–407, doi:10.1038/nature03943.
- Corbi, F., F. Funiello, C. Faccenna, G. Ranalli, and A. Heuret (2011), Seismic variability of subduction thrust faults: Insights from laboratory models, *J. Geophys. Res.*, *116*, B06304, doi:10.1029/2010JB007993.
- Corbi, F., F. Funiello, M. Moroni, Y. van Dinther, P. M. Mai, L. A. Dalguer, and C. Faccenna (2013), The seismic cycle at subduction thrusts: 1. Insights from laboratory models, *J. Geophys. Res. Solid Earth*, *118*, 1–19, doi:10.1029/2012JB009481.
- Dal Zilio, L., Y. van Dinther, and T. Geria (2016), Plate convergence rate controls earthquake-size distribution of mountain belts. AGU abstract T22B-02.
- Di Giuseppe, E., F. Funiello, F. Corbi, G. Ranalli, and G. Mojoli (2009), Gelatins as rock analogs: A systematic study of their rheological and physical properties, *Tectonophysics*, *473*(3–4), 391–403, doi:10.1016/j.tecto.2009.03.012.
- Dziewonski, A. M., and J. H. Woodhouse (1981), Determination of earthquake source parameters from waveform data for studies of global and regional seismicity, *J. Geophys. Res.*, *86*, 2825–2852, doi:10.1029/JB086iB04p02825.
- Engdahl, R., and A. Villaseñor (2002), Global seismicity: 1900–1999, in *International Handbook of Earthquake and Engineering Seismology, Part A*, edited by W. H. K. Lee et al., chap. 41, pp. 665–690, Academic, Amsterdam.
- Funiello, F., F. Corbi, Y. van Dinther, and A. Heuret (2013), Unraveling megathrust seismicity, *Eos Trans. AGU*, *94*(51), 497–504, doi:10.1029/2010JB007993.
- Gerya, T., and D. Yuen (2007), Robust characteristics method for modelling multiphase visco-elasto-plastic thermo-mechanical problems, *Phys. Earth Planet. In.*, *163*(1–4), 83–105.
- Herrendörfer, R., Y. van Dinther, T. Gerya, and L. A. Dalguer (2015), Earthquake supercycle in subduction zones controlled by the width of the seismogenic zone, *Nat. Geosci.*, *8*(6), 471–474, doi:10.1038/ngeo2427.
- Heuret, A., S. Lallemand, F. Funiello, C. Piromallo, and C. Faccenna (2011), Physical characteristics of subduction interface type seismogenic zones revisited, *Geochem. Geophys. Geosyst.*, *12*, Q01004, doi:10.1029/2010GC003230.
- Heuret, A., C. P. Conrad, F. Funiello, S. Lallemand, and L. Sandri (2012), Relation between subduction megathrust earthquakes, trench sediment thickness and upper plate strain, *Geophys. Res. Lett.*, *39*, L05304, doi:10.1029/2011GL050712.
- Ide, S. (2013), The proportionality between relative plate velocity and seismicity in subduction zones, *Nat. Geosci.*, *6*(8), 1–5, doi:10.1038/ngeo1901.
- Ide, S., G. C. Beroza, D. R. Shelly, and T. Uchide (2007), A scaling law for slow earthquakes, *Nature*, *447*(7140), 76–79, doi:10.1038/nature05780.
- Jarrard, R. D. (1986), Relations among subduction parameters, *Rev. Geophys.*, *24*, 217–284, doi:10.1029/RG024i002p00217.
- Kanamori, H., and E. E. Brodsky (2001), The physics of earthquakes, *Phys. Today*, *54*(6), 34, doi:10.1063/1.1387590.
- Kelleher, J., J. Savino, H. Rowlett, and W. McCann (1974), Why and where great thrust earthquakes occur along island arcs, *J. Geophys. Res.*, *79*, 4889–4899, doi:10.1029/JB079i032p04889.
- Lay, T., H. Kanamori, and L. Ruff (1982), The asperity model and the nature of large subduction zone earthquakes, *Earthquake Predict. Res.*, *1*, 3–71.
- Marone, C., and D. M. Saffer (2007), Fault friction and the upper transition from seismic to aseismic faulting, in *The Seismogenic Zone of Subduction Thrust Faults*, edited by T. H. Dixon and C. Moore, pp. 346–369, Columbia Univ. Press, New York.
- McCaffrey, R. (2008), Global frequency of magnitude 9 earthquakes, *Geology*, *36*(3), 263, doi:10.1130/G24402A.1.
- Noda, H., and N. Lapusta (2013), Stable creeping fault segments can become destructive as a result of dynamic weakening, *Nature*, *493*(7433), 518–521, doi:10.1038/nature11703.
- Pacheco, J. F., L. R. Sykes, and C. H. Scholz (1993), Nature of seismic coupling along simple plate boundaries of the subduction type, *J. Geophys. Res.*, *98*(B8), 14,133–14,159, doi:10.1029/93JB00349.
- Peng, Z., and J. Gombert (2010), An integrated perspective of the continuum between earthquakes and slow-slip phenomena, *Nat. Geosci.*, *3*(9), 599–607, doi:10.1038/ngeo940.
- Philibosian, B., K. Sieh, J. Avouac, D. H. Natawidjaja, H. Chiang, C. Wu, H. Perfettini, C. Shen, M. R. Daryono, and B. W. Suwargadi (2014), Rupture and variable coupling behavior of the Mentawai segment of the Sunda megathrust during the supercycle culmination of 1797 to 1833, *J. Geophys. Res. Solid Earth*, *119*, 7258–7287, doi:10.1002/2014JB011200.
- Press, W. H., S. A. Teukolsky, W. T. Vetterling, and B. P. Flannery (1996), *Numerical Recipes in C*, pp. 609–650, Cambridge Univ. Press, Cambridge, New York.
- Radiguet, M., H. Perfettini, N. Cotte, A. Gualandi, B. Valette, V. Kostoglodov, T. Lhomme, A. Walpersdorf, E. Cabral Cano, and M. Campillo (2016), Triggering of the 2014  $M_w$  7.3 Papanoa earthquake by a slow slip event in Guerrero, Mexico, *Nat. Geosci.*, *9*, 829–833.
- Romano, F., E. Trasatti, S. Lorito, C. Piromallo, A. Piatanesi, Y. Ito, D. Zhao, K. Hirata, P. Lanucara, and M. Cocco (2014), Structural control on the Tohoku earthquake rupture process investigated by 3D FEM, tsunami and geodetic data, *Sci. Rep.*, *4*, 5631, doi:10.1038/srep05631.
- Rosenau, M., J. Lohrmann, and O. Oncken (2009), Shocks in a box: An analogue model of subduction earthquake cycles with application to seismotectonic forearc evolution, *J. Geophys. Res.*, *114*, B01409, doi:10.1029/2008JB005665.
- Ruff, L., and H. Kanamori (1980), Seismicity and the subduction process, *Phys. Earth Planet. In.*, *23*(3), 240–252, doi:10.1016/0031-9201(80)90117-X.
- Schellart, W. P., and N. Rawlinson (2013), Global correlations between maximum magnitudes of subduction zone interface thrust earthquakes and physical parameters of subduction zones, *Phys. Earth Planet. In.*, *225*, 41–67, doi:10.1016/j.pepi.2013.10.001.
- Scholz, C. H. (1998), Earthquakes and friction laws, *Nature*, *391*(6662), 37–42, doi:10.1038/34097.
- Scholz, C. H., and J. Campos (2012), The seismic coupling of subduction zones revisited, *J. Geophys. Res.*, *117*, B05310, doi:10.1029/2011JB009003.
- Schwartz, S. Y., and J. M. Rokosky (2007), Slow slip events and seismic tremor at circum-pacific subduction zones, *Rev. Geophys.*, *45*, RG3004, doi:10.1029/2006RG000208.
- Shearer, P., and R. Bürgmann (2010), Lessons learned from the 2004 Sumatra-Andaman megathrust rupture, *Annu. Rev. Earth Planet. Sci.*, *38*, 103–131, doi:10.1146/annurev-earth-040809-152537.
- Sieh, K., D. H. Natawidjaja, A. J. Meltzner, C.-C. Shen, H. Cheng, K.-S. Li, B. W. Suwargadi, J. Galetzka, B. Philibosian, and R. L. Edwards (2008), Earthquake supercycles inferred from sea-level changes recorded in the corals of West Sumatra, *Science*, *322*(5908), 1674–1678, doi:10.1126/science.1163589.
- Sveen, J. K. (2004), An introduction to MatPIV v.1.6.1 Eprint no. 2, ISSN 0809-4403, Department of Mathematics, University of Oslo. [Available at <http://www.math.uio.no/jks/matpiv>.]

- Uyeda, S. (1983), Comparative subductology, EPISODES o.93 No 2.
- Uyeda, S., and H. Kanamori (1979), Back-arc opening and the mode of subduction, *J. Geophys. Res.*, *84*(B3), 1049–1061, doi:10.1029/JB084iB03p01049.
- van Dinther, Y., T. Gerya, L. Dalguer, F. Corbi, F. Funicello, and P. Mai (2013a), The seismic cycle at subduction thrusts: 2. Dynamic implications of geodynamic simulations validated with laboratory models, *J. Geophys. Res. Solid Earth*, *118*, 1502–1525, doi:10.1029/2012JB009479.
- van Dinther, Y., T. V. Gerya, L. A. Dalguer, P. M. Mai, G. Morra, and D. Giardini (2013b), The seismic cycle at subduction thrusts: Insights from seismo-thermo-mechanical models, *J. Geophys. Res. Solid Earth*, *118*, 183–6202, doi:10.1002/2013JB010380.
- van Dinther, Y., P. M. Mai, L. A. Dalguer, and T. V. Gerya (2014), Modeling the seismic cycle in subduction zones: The role of off-megathrust earthquakes, *Geophys. Res. Lett.*, *41*, 1194–1201, doi:10.1002/2013GL058886.
- Wang, K., and S. L. Bilek (2014), Fault creep caused by subduction of rough seafloor relief, *Tectonophysics*, *610*(2014), 1–24, doi:10.1016/j.tecto.2013.11.024.
- Wells, D. L., and K. J. Coppersmith (1994), New empirical relationships among magnitude, rupture length, rupture width, rupture area, and surface displacement, *Bull. Seismol. Soc. Am.*, *84*(4), 974–1002.